Calcium spikes accompany the cleavage furrow ingression and cell separation during fission yeast cytokinesis

Abhishek Poddar[1], Oumou Sidibe[1], Aniruddha Ray[2] and Qian Chen[1, *]

* Lead contact: qian.chen3@utoledo.edu

[1]: Department of Biological Sciences

[2]: Department of Physics and Astronomy

The University of Toledo

2801 West Bancroft ST

Toledo, OH, 43606

Running title: Calcium spikes during yeast cytokinesis

Abbreviations:

Keyword: cytokinesis, calcium transient, fission yeast, GCaMP

Abstract

The role of calcium signaling during cytokinesis has long remained ambiguous. The studies of embryonic cell division discovered that calcium concentration increases transiently at the division plane just before the cleavage furrow ingression, leading to the hypothesis that these calcium transients trigger the contractile ring constriction. However, such calcium transients have only been found in animal embryos and their function remains controversial. Here we explored cytokinetic calcium transients in the model organism fission yeast. We adopted GCaMP, a genetically encoded calcium indicator, to determine the intracellular calcium level. We validated GCaMP as a highly sensitive calcium indicator which allowed us to capture the calcium transients stimulated by osmotic shocks. To identify calcium transients during cytokinesis, we first identified a correlation between the intracellular calcium level and cell division. Next, we discovered calcium spikes at the start of the cleavage furrow ingression and the end of the cell separation using time-lapse microscopy to. Inhibition of these calcium spikes slowed down the furrow ingression and led to frequent lysis of the daughter cells. We conclude that like the larger animal embryos fission yeast triggers cytokinetic calcium transients which promote the ring constriction and daughter cell integrity (194).

Highlight summary for TOC:

Calcium rises transiently at the division plane during embryonic cell cytokinesis, but the conservation and function of such calcium transients remain unclear. We identified similar calcium spikes during fission yeast cytokinesis and demonstrated that these spikes promote the contractile ring constriction and the daughter cell integrity (257).

38 **Introduction**

39 Calcium is an essential secondary messenger in many cellular processes but its role during
40 cytokinesis, the last stage of cell division, remains ambiguous. Eukaryotic cells maintain their
41 intracellular calcium at much lower concentration than that of their extracellular environment. A
42 transient increase of the free calcium level, through either release from the intracellular storage
43 or influx through the plasma membrane, triggers a number of essential calcium signaling
44 pathways (for a review see (Clapham, 2007)).

45 Although the importance of calcium to cytokinesis had long been known (Arnold, 1975),
46 the calcium transients accompanying cytokinesis were discovered much later and remain poorly
47 understood. Fluck et al. first observed two localized calcium waves at the cell division plane of
48 medaka fish embryos during cytokinesis (Fluck et al., 1991). The first wave initiates just before
49 the cleavage furrow ingression while the second wave appears after the cell separation.
50 Followed-up studies discovered similar localized increase of calcium in other animal embryos,
51 including those of zebra fish *Danio rerio* and African frog *Xenopus laevis* (Chang and Meng,
52 1995; Miller et al., 1993; Noguchi and Mabuchi, 2002). However, it remains unexplored whether
53 such calcium transients are universal among all eukaryotic cells. Neither is there a consensus on
54 the exact molecular function of these transients. The prevailing hypothesis (Chang and Meng,
55 1995; Fluck et al., 1991) holds that these transients can activate myosin light chain kinase
56 (MLCK) to promote the activity of myosin II motor in the contractile ring and trigger the ring
57 constriction (Craig et al., 1983; Scholey et al., 1980). This theory draws a parallel between the
58 role of calcium in cytokinesis to that in smooth muscle constriction (Nishimura et al., 1990).
59 This proposal, although attractive, has remained unproven even in the animal embryos. Adding
60 to the ambiguity, inhibition of the cytokinetic calcium transients in *X. laevis* embryos has

61 produced conflicting results (Miller et al., 1993; Noguchi and Mabuchi, 2002; Snow and
62 Nuccitelli, 1993). To date, both the nature and molecular function of the cytokinetic calcium
63 transients remain undetermined.

64 Fission yeast *Schizosacchromyces pombe* has emerged as an excellent model organism
65 for the study of cytokinesis in the last twenty years. The molecular mechanism of cytokinesis in
66 this unicellular organism has been largely conserved in higher eukaryotes (for review see
67 (Pollard and Wu, 2010)). Like animal cells, fission yeast assembles an actomyosin contractile
68 ring at the cell division plane (Wu et al., 2003), a process mediated by essential cytokinetic
69 proteins such as Myo2p, Cdc12p and Adf1p (Balasubramanian et al., 1998; Chang et al., 1997;
70 Chen and Pollard, 2011). The assembly of contractile ring is further promoted by a continuous
71 polymerization of actin filaments in the ring (Courtemanche et al., 2016). As in higher
72 eukaryotes, the actomyosin ring constricts to drive the cleavage furrow ingression, assisted by a
73 growing septa (Laplante et al., 2015; Mishra et al., 2013). The terminal step of cell separation
74 (for review see (Garcia Cortes et al., 2016; Sipiczki, 2007) requires degradation of the septa
75 (Cortes et al., 2002; Cortes et al., 2012; Liu et al., 1999; Munoz et al., 2013) as well as proper
76 regulation of the turgor pressure (Atilgan et al., 2015; Proctor et al., 2012).

77 Although it still remains a challenge to quantify the free calcium concentration in a live
78 cell, the rapid development of genetically encoded calcium indicators (GECI) over the last
79 twenty years has made it far easier than before. Compared to the more widely used synthetic
80 probes, GECIs can be expressed in vivo without intrusive probe-loading procedure. This is
81 particularly advantageous in such genetically modifiable systems as fission yeast. Although most
82 GECIs still trail the chemical probes in their sensitivity, some of them such as GCaMP (Nagai et
83 al., 2001), which we chose for this study, have come close. This single fluorophore sensor

84 consists of three domains: a circularly permuted enhanced green-fluorescent protein (cp-EGFP),
85 a calcium-binding calmodulin motif and a M13 peptide of human myosin-light chain kinase
86 (MLCK). Binding of calcium to the calmodulin motif dissociates the M13 peptide from cp-
87 EGFP, increases the fluorescence of GCaMP significantly (Nakai et al., 2001). Further
88 modifications of GCaMP have substantially reduced its response time and enhanced its signal-to-
89 noise ratio (Chen et al., 2013; Tian et al., 2009). We picked one of the most sensitive variants,
90 GCaMP6s (Chen et al., 2013), to explore the potential calcium transients during fission yeast
91 cytokinesis.

92 Few studies have examined the calcium level of fission yeast at the single cell level, even
93 though its calcium signaling pathways have been characterized extensively. Two central
94 calcium-signaling molecules, calmodulin and calcineurin, have both been identified (Moser et
95 al., 1997; Takeda and Yamamoto, 1987; Yoshida et al., 1994). As in animal cells, they play a
96 critical role in a plethora of cellular processes including cytokinesis in fission yeast. In particular,
97 the essential calmodulin Cam1p is required for cell division, underlying the importance of
98 calcium-signaling in this model organism (Moser et al., 1997). Past studies have mostly
99 employed bulk assays to determine the average calcium level of many cells, using either
100 chemical or indirect probes (Deng et al., 2006; Ma et al., 2011). As a result, the regulation of
101 calcium at the sub-cellular level during many processes including cytokinesis has been left
102 undetermined.

103 In this study we first explored the feasibility of GCaMP-based calcium imaging in fission
104 yeast. We then deployed this probe to capture the calcium transients triggered by various stimuli
105 to validate its effectiveness. Finally, we identified the cytokinetic calcium spikes and examined
106 their importance to cytokinesis.

107 **Results**

108 **Expression and localization of the genetically calcium indicator GCaMP in fission yeast**

109 To probe the intracellular calcium level of fission yeast cells with fluorescence microscopy, we
110 expressed a single copy of the GCaMP coding sequence at an endogenous locus. A strong
111 constitutive ADH promoter drove the expression of GCaMP6s (referred to as GCaMP) (Fig. 1A).
112 To measure the expression and sub-cellular localization of this calcium indicator, we tagged its
113 C-terminus with another fluorescence protein mCherry. GCaMP-mCherry localized uniformly
114 throughout the cytoplasm and the nucleus but it was excluded from the vacuoles (Fig. 1B). The
115 reporter nevertheless was slightly enriched in the nucleus, compared to the cytoplasm (ratio = 1.5
116 ± 0.1, average ± S.D., n = 66). The ratio of GCaMP to mCherry intracellular fluorescence varied
117 very little among the cells (Fig. 1C), indicating that the expression of this reporter is
118 homogenous. We concluded that GCaMP can be expressed homogenously in the fission yeast
119 cells and this calcium indicator localizes throughout the intracellular space.

120 We next determined whether the expression of GCaMP perturbs any cellular functions, a
121 potential concern for endogenously expressed reporters. Overall the GCaMP expressing cells
122 exhibited no apparent morphological defects. Their length and width were similar to the wild-
123 type cells (Fig. 1D). Their mitotic and septation indexes were also normal, similar to the wild
124 type (Fig. 1E-F). Moreover, these GCaMP expressing cells did not exhibit any hyper-sensitivity
125 to either calcium, or sorbitol, or EGTA, all of which likely perturb the intracellular calcium
126 homeostasis (Fig. S1). Lastly, cytokinesis in these GCaMP-expressing cells were unperturbed, as
127 determined by time-lapse fluorescence microscopy. In the GCaMP-expressing cells, the
128 contractile ring assembly and maturation took 44 ± 5 mins (average ± S.D., n = 31), starting from
129 the appearance of precursor nodes, similar to the wild-type cells (43 ± 4 mins, n = 40). This was

130 followed by the ring constriction that took 30 ± 3 mins (n = 43), same as the wild type (30 ± 3
131 mins, n = 70). The last stage of cytokinesis the cell separation required 26 ± 4 mins (n = 29) in
132 the GCaMP-expressing cells, not significantly different from the wild type (25 ± 3 mins, n = 67).
133 These quantitative measurements indicated that expression of GCaMP dose not interfere with
134 cytokinesis either. Since GCaMP does not produce any discernable artifacts, we combined our
135 GCaMP-expressing strain with quantitative microscopy to examine the intracellular calcium
136 level of fission yeast cells.

137 **Calcium transients in fission yeast cells**

138 To validate GCaMP as an effective calcium indicator, we first determined whether an increase of
139 extracellular calcium alters the fluorescence of GCaMP-expressing cells. In the rich YE5s media,
140 addition of 30mM $CaCl_2$ increased average fluorescence of the GCaMP expressing cells by
141 about three folds, compared to those in YE5s (Fig. 2A-B). The increased extracellular calcium
142 concentration also resulted in more frequent fluctuations of the intracellular GCaMP
143 fluorescence (Fig. 2C-D and Supplemental Movie S1). Thus, GCaMP-based imaging is fully
144 capable of detecting alterations of calcium concentration.

145 Next, we employed the GCaMP-based time-lapse imaging to capture rapid changes of
146 intracellular calcium level, the calcium transients. The resting fission yeast cells produced only
147 sporadic calcium transients (Fig. 2C). We applied various stimuli through microfluidics to
148 produce more transients. First, we used hypo-osmotic shock, one of the best-known stimuli of
149 calcium transients in yeast (Batiza et al., 1996; Denis and Cyert, 2002). We found highly
150 synchronized calcium transients, captured by an increase of GCaMP fluorescence, in the cells
151 under such shock (Fig. 3A and Supplemental Movie S2). The intracellular calcium rose quickly
152 following the shock and peaked 2 mins after the osmotic shock on average. These calcium

153 transients accompanied the expansion of cell volume closely (Fig. 3B-C). Average amplitudes of
154 the calcium increase were proportionally to the strength of hypo-osmotic shocks (Fig. 3D).
155 Secondly, we applied hyper-osmotic shocks to the cells. This surprisingly did not elicit
156 detectable calcium transients (Fig. 3E and Fig. S2A-B). Lastly, we abrupted increased the
157 extracellular calcium concentration to stimulate the cells. This also provoked strong calcium
158 transients, but they (QC) appeared only ~5 mins after the infusion of calcium (Fig. 3F). As a
159 result of the stimulation, the average intracellular calcium concentration remained elevated after
160 more than 20 mins. This response to the external calcium shock confirmed a similar observation
161 made through the bulk assays (Deng et al., 2006). Our results demonstrated that the GCaMP-
162 based time-lapse imaging can capture the calcium transients in fission yeast cells, making it
163 entirely feasible to identify the cytokinetic calcium transients.

164 **Identification of calcium spikes during cytokinesis**

165 As the first step to determine the link between calcium and cytokinesis, we analyzed the
166 intracellular calcium level in a large number of asynchronized cells. Dividing fission yeast cells
167 can be identified through their increased length. These rod-shaped cells grow by tip extension,
168 starting to grow from a length of ~7 μm after birth. They expand throughout interphase until
169 stopping at a length of ~14 μm at the mitotic entry (Mitchison and Nurse, 1985). We found that
170 the calcium level was constant among most cells regardless of their length (n = 407) (Fig. 4A).
171 However, the calcium centration of a few cells was significantly higher than the average
172 (>110%). The length distribution of these "outliers" was interestingly bimodal. Two peak
173 fractions are ~14 μm and ~8 μm respectively (Fig. 4B), roughly equaling to the length of the
174 dividing and new-born cells respectively. The existence of the outlier cells with high calcium
175 level provided the first hint of calcium transients during cell division.

176 Next, we examined the temporal regulation of intracellular calcium in the dividing cells
177 through time-lapse microscopy. To facilitate our analysis, these cells expressed both GCaMP and
178 well-established fluorescence protein markers of cytokinesis. First, we looked closely at the
179 calcium level during mitosis, by imaging the cells expressing both GCaMP and Sad1p-GFP, a
180 marker of spindle pole bodies (SPB). In fission yeast, the separation of SPBs is concomitant with
181 the start of prometaphase and anaphase B ends ~30 mins after (Fig. S3A) (Wu et al., 2003).
182 During this period, we captured very few calcium transients. About 34 mins after the separation
183 of SPBs, the calcium level started to rise quickly throughout the intracellular space, which we
184 termed calcium spikes. These spikes appeared to be well-synchronized, coinciding with
185 telophase as well as early cytokinesis (Fig. S3B-C). Next, we determined whether these calcium
186 spikes initiated exactly at the beginning of furrow ingression as those calcium transients did in
187 the fish embryos (Chang and Meng, 1995; Fluck et al., 1991). We imaged the cells expressed
188 GCaMP and a contractile ring marker Rlc1p-tdTomato, the regulatory myosin light chain (Fig.
189 5A). Our movies recorded very few calcium spikes during the assembly and maturation of the
190 contractile ring (Fig. 5A-B). In comparison, our time-lapse microscopy consistently captured
191 calcium spikes accompanying the start of ring constriction in most dividing cells. The spikes also
192 appeared frequently during the constriction. We called them "constricting spikes" (Fig. 5B-C and
193 Supplemental Movie S3). In these cytokinetic cells, the average intracellular calcium level
194 increased ~1.7 fold within 1 ± 3 min (average ± S.D., n = 64) of the start of the cleavage furrow
195 ingression (Fig. 5D).

196 Besides the dividing cells, the intracellular calcium of new-born cells appeared to be high
197 as well, prompting us to examine the calcium spikes during cell separation. Although few
198 calcium spikes were captured following the ring closure and before the cell separation, spikes

199 were found in most cells following the cell separation (Fig. 6A). These separating spikes were
200 concomitant with the initial appearance of new ends. They distributed asymmetrically between
201 the two daughter cells (Fig. 6B-C). Among the cells (n = 73) in which at least one separating
202 spike was captured, 56% triggered the spike in only one daughter cells. The other 44% triggered
203 the calcium spikes that oscillated between the two daughter cells (Fig. 6B-C). On average, the
204 separating spikes increased the intracellular GCaMP fluorescence by ~1.7 folds (Fig. 6D-E). The
205 calcium level peaked ~2 mins after the end of cell separation (Supplemental Movie S4). We
206 observed similar constricting and separating spikes in the dividing cells inoculated in the
207 synthetic EMM5s media (Fig. S3D-E), further confirming the existence of these cytokinetic
208 spikes.

209 To better understand the spatiotemporal regulation of these cytokinetic calcium spikes,
210 we characterized them by fast imaging. We increased the frequency of time-lapse acquisition by
211 40 folds, from one frame every two minutes to one frame every three seconds. We only captured
212 a limited number of constricting and separating spikes in this way (Fig. 7A and D). Close
213 examination of the spikes found that they increased intracellular calcium level most significantly
214 at the tip, the peri-nuclear space, and the division plane (Fig. 7B and E). All of them exhibited a
215 lifespan of 50-200 seconds (Fig. 7C and F). Their amplitudes were highly variable (Fig. 7C and
216 F). Some constricting spikes exhibited a more than 10-fold increase of GCaMP fluorescence
217 above the baseline level (Fig. 7C). We concluded that the cytokinetic calcium spikes rise
218 throughout the cytoplasm and they are highly heterogeneous.

219 **Functions of the fission yeast cytokinetic calcium spikes**

220 The close temporal correlation between the calcium spikes and cytokinesis prompted us to
221 investigate whether these spikes are required for cytokinesis. To this end, we depleted the

222 extracellular calcium from the media, hypothesizing that the calcium influx contributes to the
223 spikes. The calcium depletion was only temporary to minimize the effects on the other calcium-
224 dependent processes. The cells were observed in either EMM5s media without any supplemented
225 calcium or YE5s media supplemented with low concentrations of EGTA. At such concentrations,
226 we found that EGTA did not inhibit cell growth strongly (Fig. S4A). In the calcium-depleted
227 media, the average intracellular GCaMP fluorescence decreased only slightly, ~13% in YE5s
228 plus 2 mM EGTA and ~3% in the calcium-free EMM5s media (Fig. 8A-B). However, the
229 fraction of outlier cells decreased significantly under either condition (Fig. 8A-B). Although the
230 calcium spikes were no longer as visible under either conditions, quantitative image analysis
231 revealed that the total number of cytokinetic spikes was not reduced eve though their amplitudes
232 decreased dramatically (Fig. 8C-D and Fig. S4B-E). We concluded that the cytokinetic calcium
233 spikes can be inhibited by depleting extracellular calcium from the media.

234 We next examined cytokinesis in the cells whose calcium spikes are inhibited through
235 time-lapse microscopy. We found that the assembly and maturation of the contractile ring took
236 slightly longer time in the calcium-free EMM media, compared to the EMM media (Fig. 9A and
237 C). However, constriction of the contractile ring slowed down much more dramatically (30%,
238 Fig. 9E and Supplemental Movie S5). Similarly, 1-2 mM EGTA did not alter the assembly and
239 maturation of the ring significantly (Fig. 9B and D) but the constriction rate was inhibited by
240 EGTA in a dosage-dependent manner. The rate was down ~50% in YE5s plus 2mM EGTA,
241 compared to YE5s (Fig. 9E). When EGTA concentration was further increased to 5mM, most
242 contractile ring (90%, n = 30) disintegrated without completing the constriction (Fig. S5A-B).
243 We also examined the cell separation when the calcium spikes are inhibited. Surprisingly, the
244 duration of cell separation remained normal when the extracellular calcium was depleted (Fig.

245 S5C-D). Although no daughter cells lysed in the calcium-free EMM5s media, 2 mM EGTA
246 induced more than one third (35 ± 5 %, n = 103) of the daughter cells to lyse following the
247 separation (Fig. 9G-H). More cells lysed when the concentration of EGTA increased to 5 mM
248 (data not shown). Further depletion of intracellular calcium by deletion of *pmr1* resulted in 54%
249 of daughter cells lysed in the calcium-free EMM5s media even though no mutant cells lysed in
250 the regular EMM5s. Pmr1p is a ER calcium ATPase that replenish the internal storage of
251 calcium (Cortes et al., 2004). We concluded that the cytokinetic calcium spikes also likely
252 promote the integrity of separating cells.

253 **Discussion**

254 Overall, we demonstrated that GCaMP-based imaging will allow fission yeast to serve as a
255 powerful model organism for the study of calcium transients during various cellular processes.
256 Using this method, we discovered the cytokinetic calcium spikes in this unicellular model
257 organism for the first time. These calcium transients are similar to those first uncovered in
258 animal embryos. They likely play a critical role in promoting the ring constriction and the
259 daughter cell integrity.

260 **GCaMP-based calcium imaging of fission yeast**

261 To our knowledge, our study is the first one to examine the feasibility of GCaMP-based calcium
262 imaging in fission yeast cells. We are fortunate that fission yeast is quite tolerant to the
263 expression of this calcium indicator. It does not perturb many cellular processes that we
264 examined even when it is expressed constitutively. More importantly, GCaMP is also highly
265 sensitive as a probe for time-lapse microscopy, allowing us to capture calcium transients at
266 relatively low sampling rate. Compared to synthetic calcium probes, GCaMP exhibited two key
267 advantages in fission yeast. First, unlike the synthetic probes such as Calcium Green (Chang and

268 Meng, 1995), the intracellular concentration of GCaMP can be maintained at a constant level
269 through the homogenous expression. Combined with quantitative microscopy, this largely
270 eliminated the heterogeneity of fluorescence intensities among cells. In contrast, intracellular
271 concentration of the synthetic probes can be highly variable among cells. This advantage was
272 exemplified by the identification of outliers with high calcium among a large number of cells.
273 The other advantage of GCaMP is its more uniform sub-cellular localization, compared to the
274 synthetic probes. This allows detection of calcium transients throughout the cytoplasm as well as
275 the nucleus.

276 When combined with yeast genetics, GCaMP can be a very versatile tool for studying
277 calcium signaling. As an example, we constructed both GCaMP and GCaMP-mCherry for this
278 study, both of which have the potential to be employed in the future studies. We employed
279 GCaMP not GCaMP-mCherry throughout this study, primarily to preserve the spectrum for
280 imaging the fluorescence protein markers of cytokinesis. Nevertheless, the tandem reporter can
281 be used for ratio-metric imaging of intracellular calcium, potentially providing higher signal to
282 noise ratio. Overall, application of GCaMP shall make fission yeast an excellent model organism
283 to study calcium transients and homeostasis in non-excitable cells.

284 **Evolutional conservation of the cytokinetic calcium transients**

285 Our study provides fresh evidences for the existence of calcium transients in an unicellular
286 organism. Similar to the earlier studies (Chang and Meng, 1995; Fluck et al., 1991; Noguchi and
287 Mabuchi, 2002), we employed live fluorescence microscopy to determine the temporal
288 correlation between the calcium transients and cytokinesis. With the availability of fluorescence
289 protein markers of cytokinesis, we now determined the temporal regulation of these spikes with
290 more precision. In addition to time-lapse microscopy, we sought out an alternative approach to

291 illustrate this close correlation. We analyzed just snapshots of many GCaMP-expressing cells to
292 reveal the relationship between cell division and intracellular calcium level. Compared to the
293 movies, the snapshots examined all cells regardless of their cell-cycle stage, presenting a less
294 biased view of the potential calcium change in them. Combined with the previous studies of
295 animal embryos, our results strongly support that a temporal increase of calcium during
296 cytokinesis may be evolutionally conserved.

297 The temporal regulation of fission yeast cytokinetic calcium spikes bears strong
298 similarities to those found in the animal embryos. The constricting spikes of fission yeast are
299 comparable to the first "furrowing wave" observed in the animal embryos (Fluck et al., 1991)
300 which initiates just as the cleavage furrow starts to ingress (Chang and Meng, 1995; Noguchi and
301 Mabuchi, 2002). The separating spikes are comparable to the second "zipping wave" of the
302 embryos, starts just when the two daughter cells separate (Fluck et al., 1991; Noguchi and
303 Mabuchi, 2002). Both the calcium waves in the embryos and the spikes in fission yeast can last
304 for minutes, far longer than other known calcium transients (Jaffe and Creton, 1998). Although
305 no calcium spikes have been identified yet during budding yeast cytokinesis, Carbo et al.
306 observed higher frequency of calcium bursts during G1 to S phase transition in synchronized
307 cells (Carbo et al., 2017), which may be similar to the separating calcium spikes in of fission
308 yeast. Overall, our study suggests that the regulatory mechanism of calcium during cytokinesis
309 may have been conserved as well.

310 There are also key differences between the calcium spikes and those embryonic calcium
311 waves. Chief among them is the spatial regulation of these calcium transients. In fission yeast,
312 the calcium spikes propagate globally throughout the cytoplasm and nucleus. In contrast, the
313 calcium waves of animal embryos are restricted to the cleavage furrow (Chang and Meng, 1995;

314 Fluck et al., 1991) or its surrounding region (Noguchi and Mabuchi, 2002). This difference may
315 be due to varying sensitivity of the calcium probes. It is more likely that this distinction is due to
316 the relatively small size of fission yeast cells, measuring only 4 μm wide and 14 μm long,
317 compared to the embryos of hundreds of microns. So far, we found no evidence that the
318 constricting spike of fission yeast triggers the contractile ring constriction, even though there are
319 evidences that the furrowing waves trigger the ring constriction (Chang and Meng, 1995; Fluck
320 et al., 1991; Miller et al., 1993). Lastly, the asymmetry and oscillation of the separating spikes
321 are also unique to fission yeast. The oscillating behavior of the spikes is particularly striking. It
322 may be linked to the unbalanced turgor pressure between the two daughter cells during the
323 separation.

324 **Mechanism of the calcium spikes and their potential roles**

325 Although the regulatory mechanism of these cytokinetic calcium spikes remains to be explored,
326 our data suggests that they likely draw calcium from both the influx and internal release.
327 Inhibition of the influx through depleting extracellular calcium significantly inhibited the spikes
328 but not completely. Under such condition, the cytokinetic calcium spikes still occurred albeit
329 with greatly diminished amplitudes. This points to the ER- or vacuole- stored calcium as the
330 other likely sources for the spikes. Supporting this hypothesis is our observation that EGTA
331 exhibited a stronger inhibitory effect to cytokinesis, compared to the calcium-free EMM
332 medium. EGTA may have chelated the intracellular calcium slowly over long-term incubation.
333 This is consistent with the lysis of *pmr1Δ* mutant cells in the calcium-free medium. In
334 comparison, the embryonic calcium waves draw only from the internal store (Chang and Meng,
335 1995; Miller et al., 1993). It remains unclear what are the ion channels mediating the cytokinetic
336 calcium transients. Fluck et al. has first proposed the potential role of tension-sensing calcium

337 channels which can be activated during cytokinesis (Fluck et al., 1991). This remains a feasible
338 mechanism considering increased membrane tension on the cleavage furrow. Release of internal
339 calcium could be through the store-operated calcium release (SOCE) channels (Chan et al., 2016;
340 Chan et al., 2015). Nevertheless, none of these cytokinetic ion channels has been identified.

341 It remains unknown how the calcium spikes promote the contractile ring constriction and
342 the daughter cell integrity. One likely explanation is that a transient increase of intracellular
343 calcium may increase the activity of type II myosin in the ring through the phosphorylation of
344 myosin regulatory light chain (Chang and Meng, 1995; Fluck et al., 1991). Alternatively, the
345 spikes could stimulate the septum biosynthesis through activating the calcium-dependent
346 calcineurin (Cadou et al., 2013; Martin-Garcia et al., 2018; Yoshida et al., 1994). Lastly, the
347 calcium spikes may adjust the turgor pressure which is required for the separation (Abenza et al.,
348 2015; Proctor et al., 2012). Further studies will be required to determine the mechanism of
349 calcium signaling during cytokinesis.

350 **Experimental procedures**

351 **Yeast genetics**

352 We followed the standard protocols for yeast cell culture and genetics. Tetrads were dissected
353 with a Spore+ micromanipulator (Singer, UK). Yeast cells were transformed with the lithium-
354 acetate method. The pmr1Δ mutant is a commercially available fission yeast deletion library
355 (Bioneer, South Korea). All the strains used in this study are listed (Table 1).

356 To construct the GCaMP expressing strain, we amplified the coding sequence from
357 *pCMV-GCaMP6s* (Addgene, Plasmid #40753) through PCR using primers P589 and P590. The
358 DNA fragment was subcloned into a previously described plasmid *pFA6a-KanMX6-Padh1-*
359 *Tadh1* (Chen and Pollard, 2013). The GCaMP6s ORF, together with the Adh1 promoter and
360 terminator, were integrated into the *leu1* locus through PCR-based homologous recombination

361 using primers P413 and P414 (Bahler et al., 1998). The resulting strain was confirmed through
362 both PCR using primers P589 and P416 and the Sanger sequencing using primer P668. The
363 GCaMP-mCherry strain was constructed through homology-based PCR using primers P647 and
364 P648. The genome locus was sequenced to confirm the insertion of mCherry coding sequence.

365 **Fluorescence microscopy**

366 For time-lapse microscopy, the cells were first inoculated in liquid YE5s media at 25°C for two
367 days before they were harvested during the exponential growth phase at a density between
368 $5*10^6$/ml to $1.0*10^7$/ml. 20 µl of the cell culture were spotted onto the glass-coverslip (#1.5) in a
369 10 mm petri dish (Cellvis, USA). The coverslip was pre-coated with 50µl of 50-100 µg/ml of
370 lectin (Sigma, L2380) and allowed to dry for 3-4 hours in a 30°C incubator. After 10 min at
371 room temperature, most cells attached to the coverslip in the petri dish. 2ml of YE5s media was
372 then added to the dish before microscopy. When chelation of calcium in media is required, 2ml
373 of YE5s supplemented with EGTA was added instead.

374 For the experiments in the calcium-free media, we prepared the synthetic EMM media by
375 omitting $CaCl_2$ (100µM) and replacing calcium pantothenate (Vitamin B5) with sodium
376 pantothenate (Cayman Chemical, Cat# NC1435671). The cells were first inoculated in YE5s
377 media for 1 day, followed by another ~15 hours in EMM5s. After harvesting the exponentially
378 growing cells, we washed them three times with the calcium-free media before proceeding to
379 microscopy.

380 We employed a spinning disk confocal microscope for the time-lapse microscopy. The
381 microscope is an Olympus IX71 unit equipped with a CSU-X1 spinning disk unit (Yokogawa,
382 Japan). The motorized stage (ASI, USA) includes a Piezo Z Top plate for acquiring Z-series. The
383 images were captured on an EMCCD camera (IXON-897, Andor) controlled by iQ3.0 (Andor).

384 Solid-state lasers of 488 nm and 561 nm were used in the fluorescence microscopy, at power of
385 no more than 2.5mW. Unless specified, we used a 60x objective lens (Olympus, Plan
386 Apochromat, NA = 1.40). Typically, a Z-series of 8 slices at an interval of 1 μm was captured at
387 each time point during the time-lapse microscopy. The temperature was maintained at ~22 ± 2°C
388 in a designated room for microscopy. To further minimize environmental variations, we typically
389 imaged both control and experimental groups with randomized order in the same day.

390 For visualization of septum, we fixed the cells with 4% formaldehyde (EMS, USA)
391 before staining them with 1 μg/ml of calcofluor white (Sigma, Cat# 18909). For visualization of
392 nuclei, we fixed the cells with 70% cold ethanol before staining them with 1 μg/ml DAPI
393 (Roche, Cat# 1023627001). To image fixed cells, we used an Olympus IX81 microscope
394 equipped with a XM10 camera and a mercury lamp.

395 To apply osmotic and calcium stresses, we used a CellASIC ONIX2 system (EMD
396 Millipore), controlled by a desktop computer through the software ONIX (EMD Millipore). To
397 trap cells in the imaging chamber of a microfluidics plate (Y04C), we injected the exponentially
398 growing cell culture to the chamber at a pressure of 34.5 KPa for 2 mins, followed by a
399 continuous infusion of YE5s media at a pressure of 10KPa for another 30 mins. To apply hyper-
400 osmotic stresses, we injected YE5s plus sorbitol into the chamber at a pressure of 10 KPa.
401 Similarly, to apply hypo-osmotic stresses, we injected YE5s into the chamber at a pressure of 10
402 KPa after the chamber had been equilibrated with a continuous infusion of YE5s plus sorbitol for
403 30 mins.

404 We captured the kinetics of cytokinetic calcium spikes by taking time-lapse microscopy
405 of the GCaMP-expressing cells at a frequency of 0.33 frame/sec without the Z-series. A
406 complete spike is defined as one with a single peak rising from and decaying to the baseline

407 level. For the constricting spikes, we examined the dividing cells with either two separating
408 nuclei or a constricting ring.

409 **Image processing and analysis**

410 We quantified the intracellular fluorescence of a GCaMP expressing cell as the total fluorescence
411 intensity of the cell divided by its area. This value was used to represent the intracellular calcium
412 level throughout the study. Cells were segmented manually, and their fluorescence intensities
413 were quantified using average intensity projections of the Z-series. The intracellular fluorescence
414 of the cells trapped in a microfluidics chamber was quantified by subtracting their combined
415 fluorescence with the background fluorescence of the camera. Unless specified, we normalized
416 the intracellular fluorescence of a cell against the baseline value, which is typically defined as the
417 average of the five lowest values recorded during a time course. The microscopy images
418 acquired during osmotic or calcium shocks were analyzed by quantifying two regions of interest
419 in cytoplasm, each measuring 1 μm in diameter. The statistics tests were done using Excel. In
420 most cases, two-tailed Student T-test was used. Standard deviations (S.D.) are used throughout
421 the study to represent data deviations.

422 For quantification of the amplitudes and number of cytokinetic calcium spikes, we first
423 segmented the dividing cells manually using NIH ImageJ. These videos are first pre-processed
424 using a median filter to reduce noise. This non-linear filter helps smoothen the images while
425 preserving high spatiotemporal resolutions. Following the noise removal, the background
426 fluorescence signal from the cells is eliminated by subtracting the temporal average of each pixel
427 in every frame. This process enables us to retain most of the flickering events, while eliminating
428 the background fluorescence to a large extent. The average fluorescence intensity of a cell is then
429 calculated by applying a binary mask on the images. Binarization of the median filtered images

430 are performed by using Otsu's thresholding method and applied to the background subtracted
431 images. The average fluorescence intensity value at each time point is then recorded and used for
432 analysis. Prior to identifying the peaks, we perform a temporal averaging of the signal, using two
433 consecutive time points, to eliminate the small fluctuations within the data. Further thresholding
434 of the signal is performed by nullifying the values lower than the temporal average of the entire
435 signal. The temporal average is used as one of the criterions to distinguish the peaks from
436 background fluctuations. This thresholding step removes the variation in the remnant background
437 fluorescence signal inside the cells. The peaks or local maxima are detected by calculating the
438 derivative at each point and identifying the points corresponding to the inversion of the
439 derivatives from positive to negative. The location and average fluorescence intensity values of
440 each individual peaks are then recorded. The video processing and analysis was performed using
441 MATLAB (Mathworks, MA).

442 To measure the rate of the contractile ring closure, we determined the duration of the ring
443 closure through analyzing the fluorescence kymograph of contractile ring. The closure rate was
444 then calculated by dividing the initial circumference of the ring before the constriction by the
445 duration. We used Image J (NIH) and custom-made macros for all the image analyses. The
446 images were first corrected for X-Y drift using the Image J StackReg plug-in (Thevenaz et al.,
447 1998) if necessary. Most plots were made with Kaleidagraph (Synergy, PA) except for the 3D
448 plots which were made with OriginLab (OriginLab, MA). The figures were made with Canvas
449 (ACDSee Systems).

450 **Acknowledgement:**

451 QC conceptualized the study, QC and AP designed and carried out the experiments, QC, AP, OS,
452 and AR analyzed the data, QC and AP wrote the manuscript.

The authors would thank Debatrayee Sinha, Mamata Malla, Zachary Kreais and Somaiyeh Khoubafarin for their technical help. They would also like to thank our colleagues at the University of Toledo Song-Tao Liu, William Taylor and Rick Komuniecki for suggestions. They would thank Dimitris Vavylonis (Lehigh University) and Ann Miller (University of Michigan) for thoughtful discussions. This work has been supported by the University of Toledo startup fund (QC), NIH R15GM134496 (QC) and DeArce-Koch Memorial Fund (QC).

Figure 1

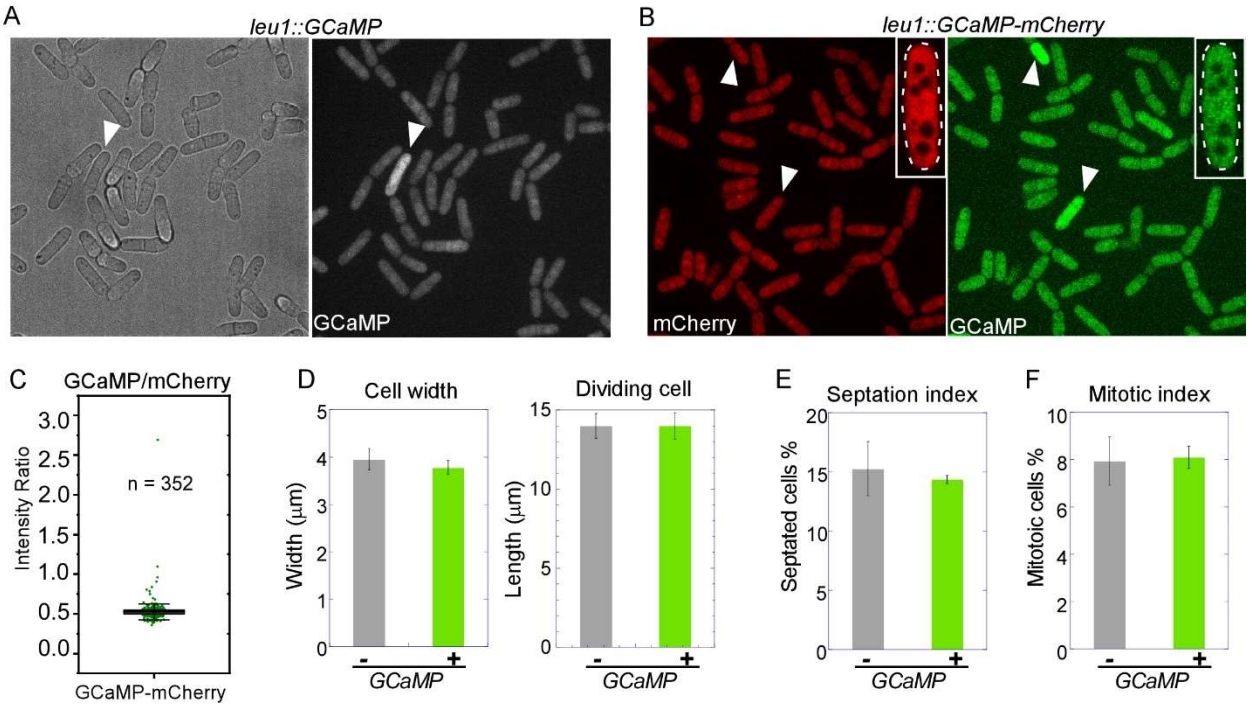

Figure 1. Expression and localization of GCaMP in fission yeast. (A) Bright-field (left) and fluorescence (right) micrographs of the cells expressing GCaMP. The intracellular fluorescence was constant for most cells, except for one outlier (white arrowhead). **(B-C)** Localization and expression of GCaMP-mCherry. **(B)** Fluorescence micrographs of the cells expressing GCaMP-mCherry. The insert shows the center slice of the Z-series of a representative cell (magnified, outlined in dashed lines). The intracellular fluorescence of mCherry remained low even in two cells with high GCaMP fluorescence (white arrow heads). GCaMP localized throughout the cytoplasm and nucleus, but it was excluded from the vacuoles. Similar results were found in three biological repeats. **(C)** A box plot showing the ratio of GCaMP:mCherry fluorescence. The expression is homogenous among the cells, resulting in a near uniform ratio with a few outliners with likely high calcium level. **(D-F)** Expression of GCaMP did not produce discernable artifacts. Bars graphs compare the GCaMP-expressing cells to the wild type. **(D)** The width of all cells (left, n > 50) and length (right, n > 50) of dividing cells. No significant differences were found (P > 0.1). **(E-F)** (D) Mitotic index (n > 1000) and (E) septation index (n > 700). No significant differences were found (P > 0.1). The data was from two biological repeats.

Figure 2

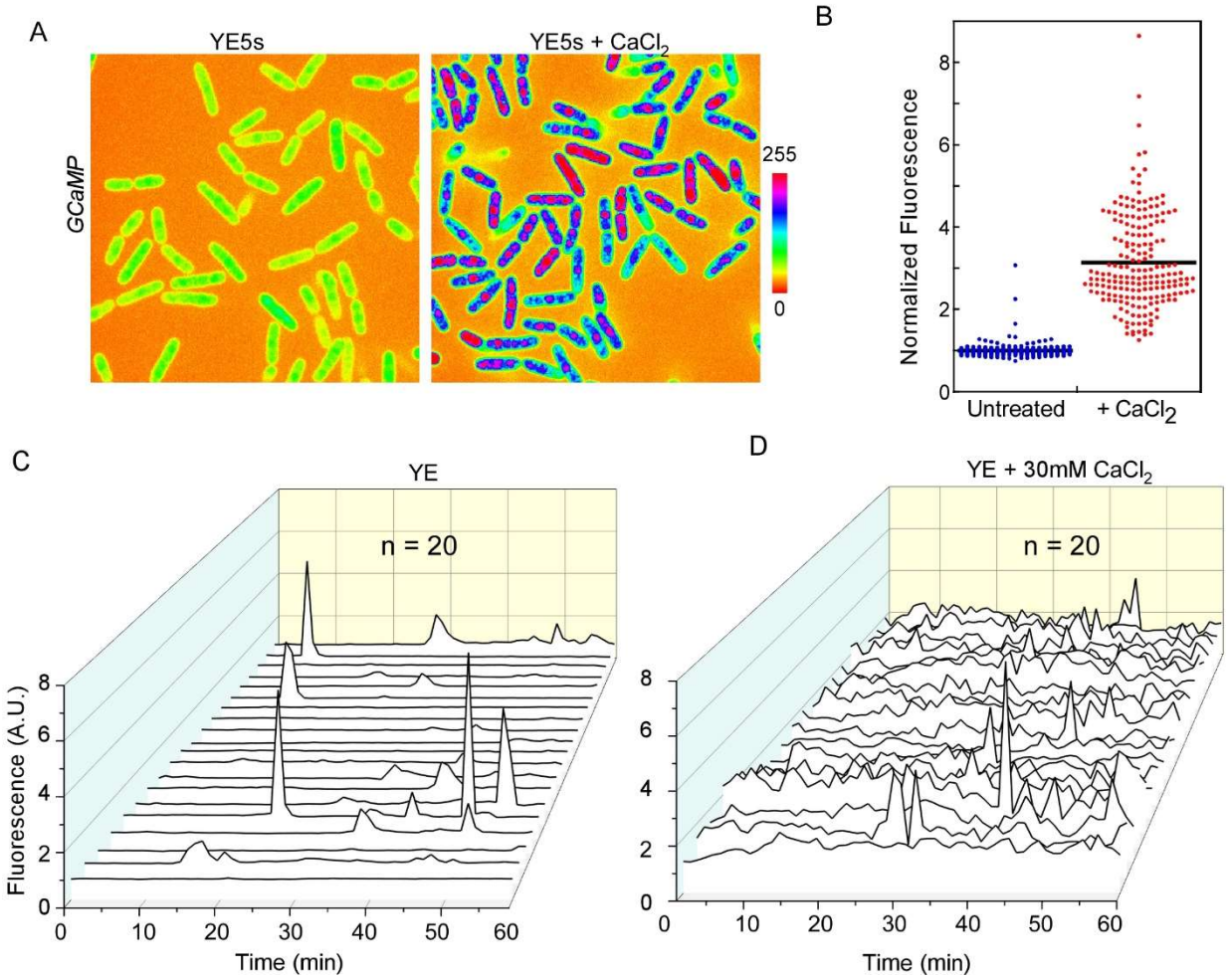

Figure 2. GCaMP responds to the calcium level increase. (A-B) The intracellular GCaMP fluorescence increased with added calcium in the media. **(A)** Fluorescence micrographs (spectrum colored) of the GCaMP-expressing cells in either YE5s (left) or YE5s supplemented with 30mM $CaCl_2$ (right). Bar represents the intensity scale. **(B)** Dot plot of fluorescence intensities of the cells (n > 190). Black line represents the average. Added calcium increased the average intracellular fluorescence by ~3 folds. **(C-D)** Calcium homeostasis of fission yeast cells. 3D-line plots show the time courses of intracellular GCaMP fluorescence in either YE5s (C) or YE5s plus 30mM $CaCl_2$ (D). The time-lapse movies were recorded at a frequency of 1 frame/min. Increased calcium in the media resulted in more frequent fluctuations of the intracellular calcium level. The data was pooled from two biological repeats.

Figure 3

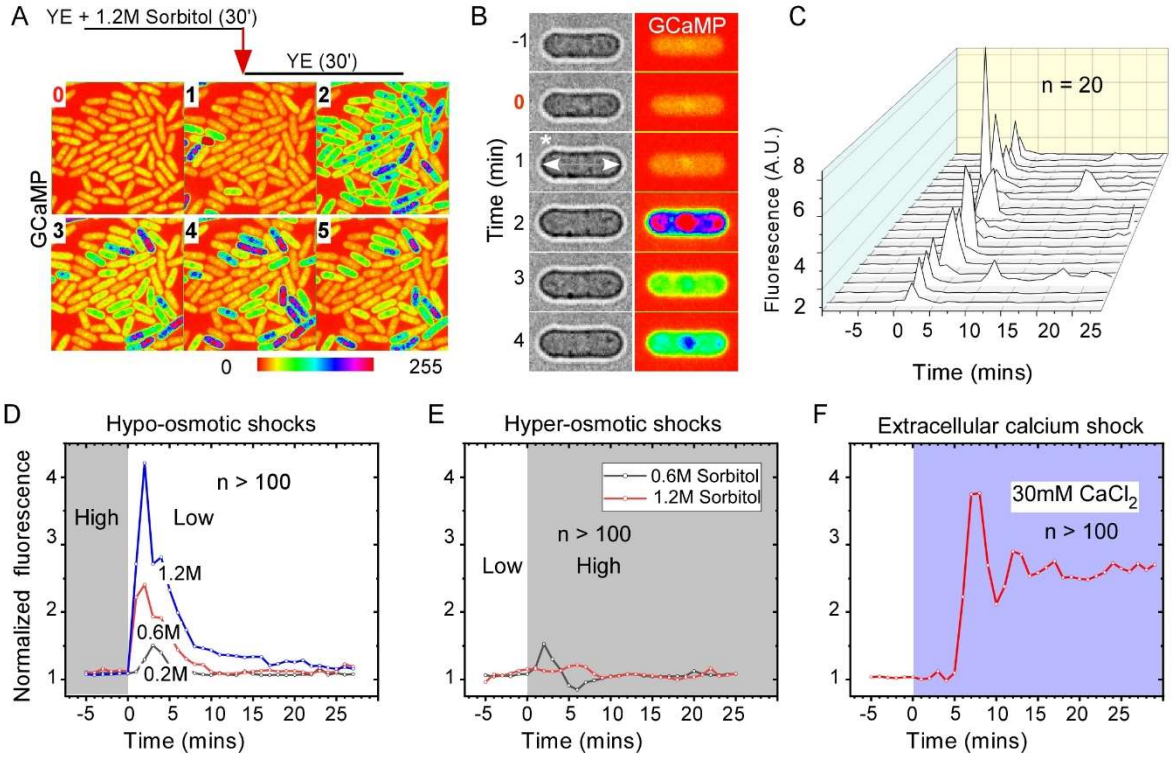

Figure 3. Osmotic shocks trigger calcium transients. (A-C) Hypo-osmotic shock triggered calcium transients in fission yeast cells. The GCaMP expressing cells, trapped in a microfluidic chamber, were first equilibrated in YE5s supplemented with 1.2M sorbitol for 30 mins before the infusion of YE5s (time zero). **(A)** Time-lapse micrographs (spectrum-colored) of a representative field in the chamber. The hypo-osmotic shock triggered a synchronized calcium spike in the cells. **(B)** Time-lapse micrographs of a representative cell. In the media with 1.2M sorbitol, the cells appeared shrunk. After the shock (time zero), the cell quickly expanded (asterisk), followed by calcium transient (right, spectrum-colored). Number: time in minutes. **(C)** 3D-line plots of the time courses of GCaMP fluorescence in twenty representative cells. The shock triggered synchronized calcium transients in every cell. Representative results from two biological repeats are shown. **(D-F)** Average time courses of the intracellular GCaMP fluorescence during either hypo-osmotic (D), or hyper-osmotic (E), or extracellular calcium (F) shocks applied through microfluidics. These stimuli triggered distinct change of intracellular calcium. **(D)** The cells were first equilibrated in YE5s with various concentrations of sorbitol for 30 mins before the infusion of YE5s media (time zero). The average amplitudes of calcium level increase were proportional to the strength of the shocks. **(E)** The cells were first equilibrated in YE5s media for 30 mins before the infusion of YE5s media supplemented with various concentrations of sorbitol (time zero). No significant change of calcium was triggered by hyper-osmotic shock. **(F)** The cells were equilibrated in YE5s media for 30 mins before the infusion of YE5s plus 30mM $CaCl_2$ (time zero). The addition of extracellular calcium triggered a delayed increase of intracellular calcium. All data is pooled from two biological repeats.

Figure 4

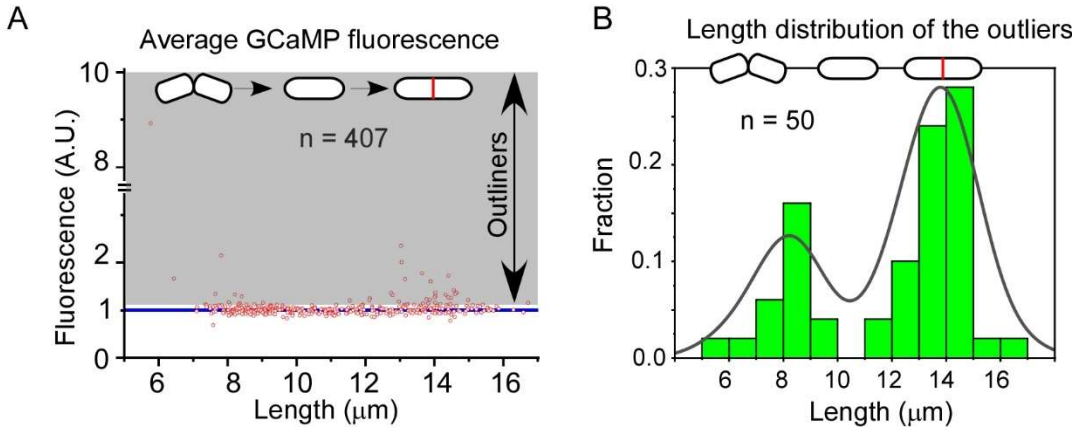

Figure 4. Correlation between intracellular calcium level and cell division. The intracellular calcium level in asynchronized cells, based on the GCaMP fluorescence. Top: cartoon representations of fission yeast cells at birth, growth, and division. **(A)** A scatter plot showing the relationship between the intracellular calcium level and the cell length. The calcium level of most cells was uniform (blue line). Only a few outlier cells (50/407) exhibited elevated (shaded area, >110% of the average) calcium level. **(B)** A histogram showing the distribution of the cell length among the outliers. The black line represents the best fit of a bimodal distribution. Two peak fractions represent the cells of 8-9 μm, and those of 14-15 μm, roughly corresponding to newly-born and dividing cells respectively. The data is pooled from four biological repeats.

Figure 5

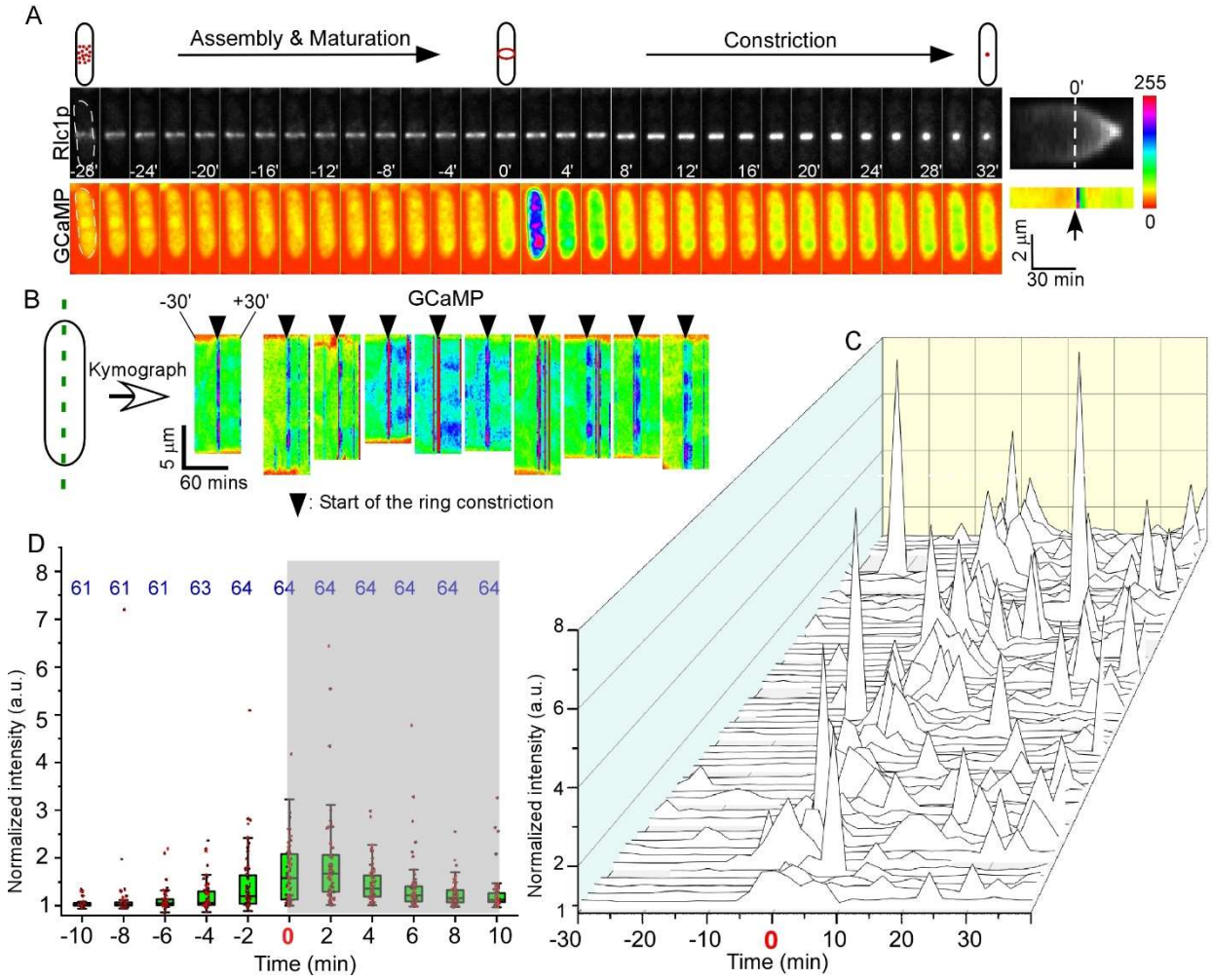

Figure 5. Calcium spikes accompany the cleavage furrow ingression. (A-B) The calcium spikes accompanied the contractile ring constriction. **(A)** Left: Time-lapse micrographs of a dividing cell expressing both Rlc1p-tdTomato (gray, top) and GCaMP (spectrum-colored, bottom). Number: time in minutes after the start of ring constriction. Interval = 2 mins. Right: Kymograph of the contractile ring (top) and the GCaMP fluorescence, with the dash line marking the start of ring constriction. A calcium spike initiated at time zero and peaked at +2 min. Bar represents the relative scale of intracellular calcium level. **(B)** Kymographs of GCaMP fluorescence in ten representative cells from -30 mins to +30 mins, relative to the initiation of ring constriction. **(C-D)** Quantitative analysis of the intracellular calcium level during the ring constriction. Data is pooled from three biological repeats. **(C)** 3-D line plots showing the time courses of calcium level in representative cells (n = 64). **(D)** Box plots of intracellular calcium level in the cells shown in C. The number on top indicates the number of observations made at each time point. The start of ring constriction was accompanied by emergence of calcium spikes. The average intracellular calcium level started to increase significantly at -4 mins and peaked at +2 mins, relative to the start of ring constriction.

Figure 6

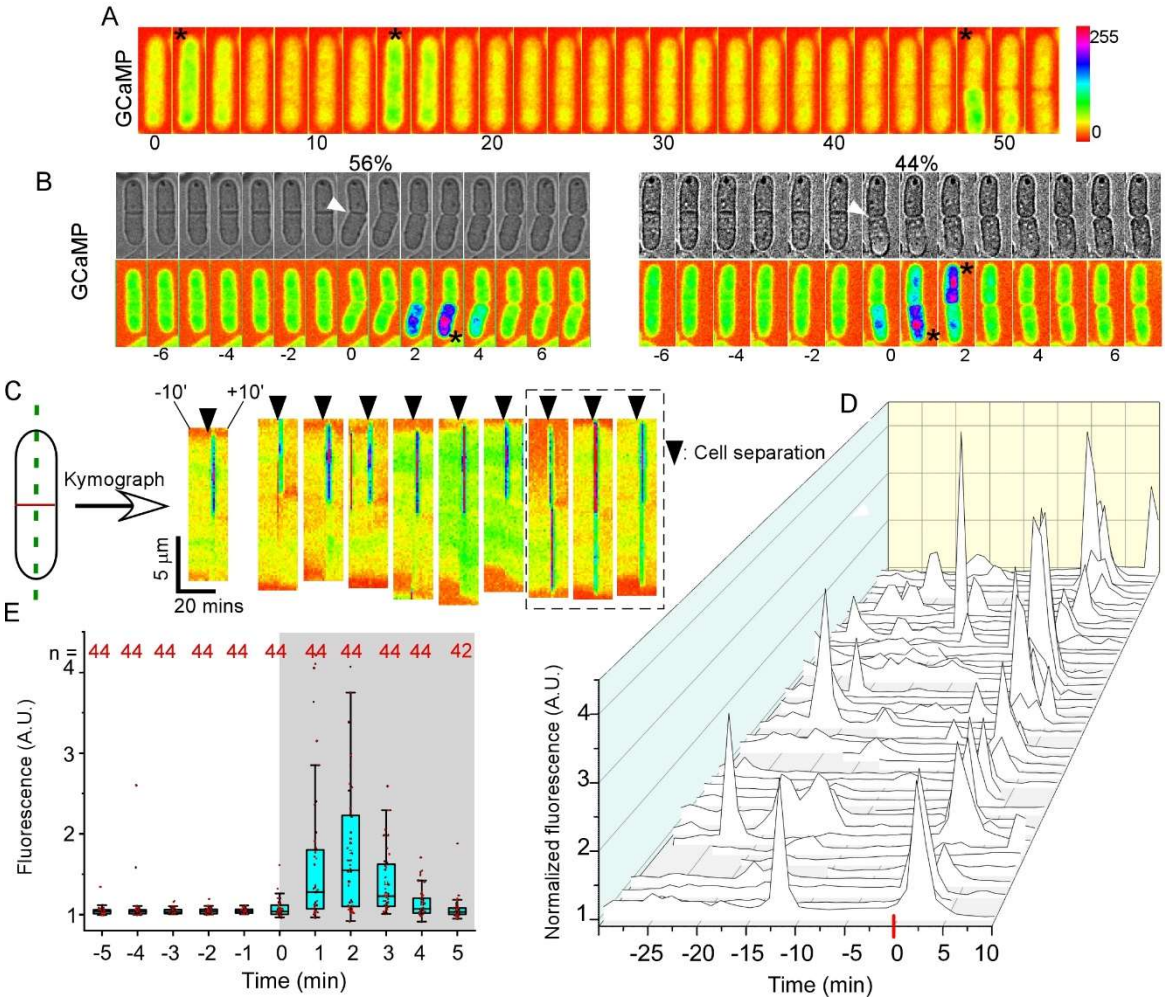

Figure 6. Calcium spikes accompany the cell separation. (A-C) Cytokinetic calcium spikes during cell separation (white arrowhead). Asterisk: the peak of a spike. Bar: the relative scale of intracellular calcium level. **(A)** Time-lapse micrographs of a cell expressing both GCaMP (spectrum-colored) and Rlc1p-tdTomato (not shown). Three calcium spikes (asterisk) are detected in this cell, including one following the start of ring constriction (time zero), the second one during the ring constriction and the third one after the cell separation (arrowhead). Number: time in minutes. Interval = 2 mins. **(B)** Time-lapse micrographs of two cells expressing GCaMP (bottom). Interval = 1 min. Number: time in minutes after the cell separation (time zero, arrowhead). The spikes appeared either in just one daughter cell (top) or oscillate between two daughter cells (bottom). Arrowhead: completion of the cell separation. (**C)** Kymograph of separating spikes in ten representative cells. Dashed box: the separating spikes oscillating between two daughter cells. **(D-E)** Quantification of the intracellular calcium level during the separation. The time-lapse movie was captured at a frequency of 1 frame/min. The data is pooled from four biological repeats. **(D)** 3-D line plots showing the time courses of intracellular calcium level in the dividing cells (n = 44). A highly synchronized calcium spike followed the cell separation (time zero) in most cells. **(E)** Box plots of the calcium level of the cells shown in D. Number of observations at each time point is indicated on the top. The average calcium level started to increase at 0 min and peaked at +2 min.

Figure 7

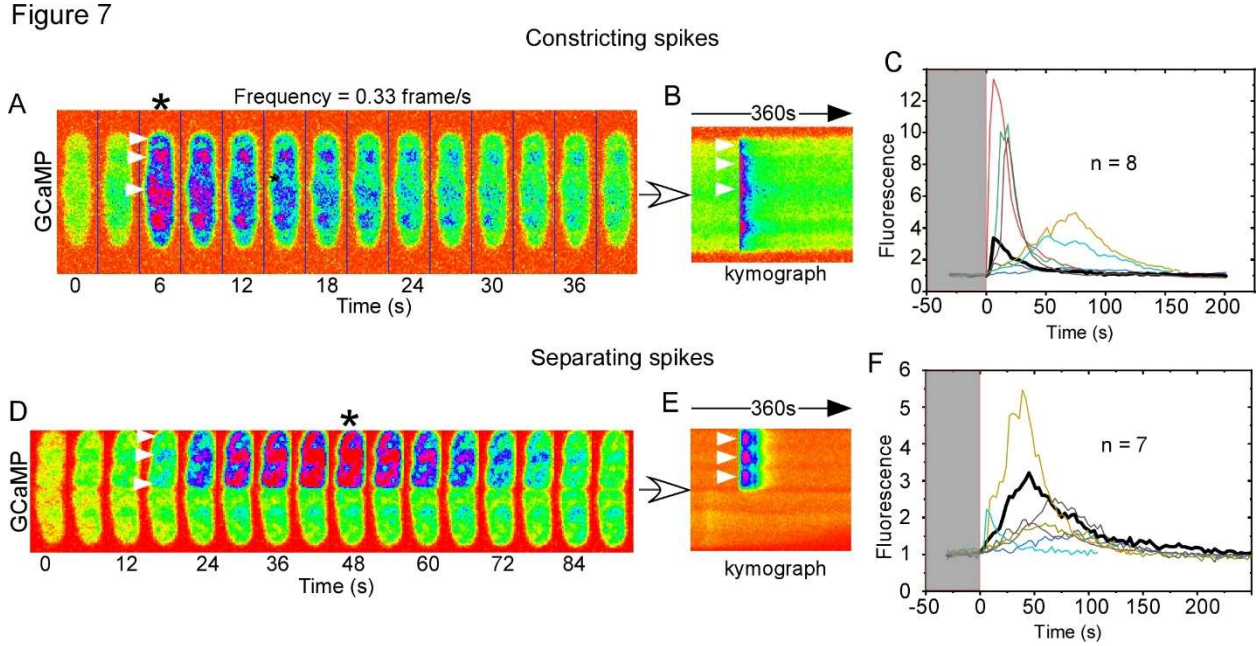

Figure 7. Spatiotemporal regulation of cytokinetic calcium spikes. The spikes were captured at a frequency of one frame every three seconds during the time-lapse microscopy. Representative constricting (A-C) or separating spikes (D-F) are shown. **(A, D)** Time-lapse micrographs (spectrum-colored) of two GCaMP-expressing cells during cytokinesis. Arrowhead: hots spot of calcium increase in the cytoplasm. Number: time in seconds after the initial rise of calcium (Time zero). Asterisk: the peak of calcium level. **(B, C)** Fluorescence kymograph of the spikes. Calcium increased most significantly at the cell tips, the peri-nuclear area and the cell division plane during spikes. **(C, F)** Time course of cytokinetic spikes including the one shown on the left (thick black line). The cytokinetic calcium spikes are highly heterogeneous with various amplitudes and lifespans. Data is pooled from three biological repeats.

Figure 8

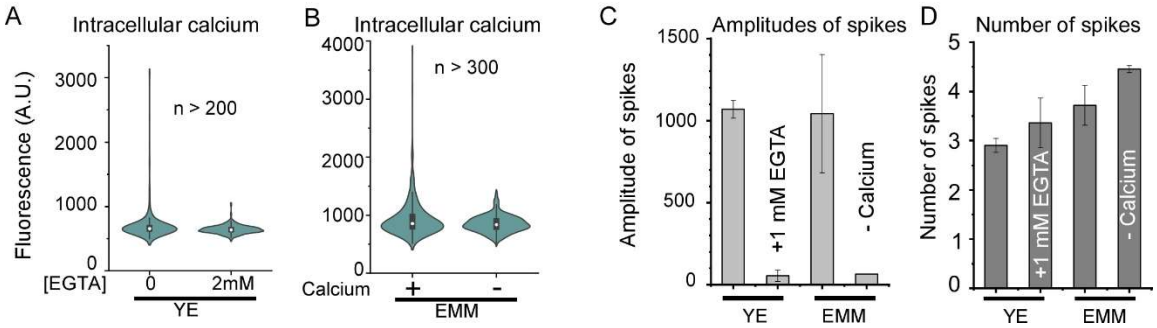

Figure 8. Depletion of extracellular calcium inhibits the cytokinetic calcium spikes. Either supplement of EGTA or removal of calcium from the media inhibited the calcium spikes. **(A-B)** Violin plots showing the intracellular calcium level in the cells. Depletion of calcium from the media reduced the average intracellular calcium level only slightly (13% by EGTA and 3% by the calcium-free EMM media) but it greatly reduced the number of outlier cells with high calcium level. **(C-D)** Bar graphs showing the average amplitude (E) and number (F) of calcium spikes during the ring constriction (n = 20). The amplitude and number of spikes are quantified through thresholding using custom-written algorithm as described in the Materials and Methods. Depletion of extracellular calcium reduced the average amplitude of calcium spikes significantly ($P < 0.001$), but not the number of peaks. The data is pooled from two biological repeats.

Figure 9

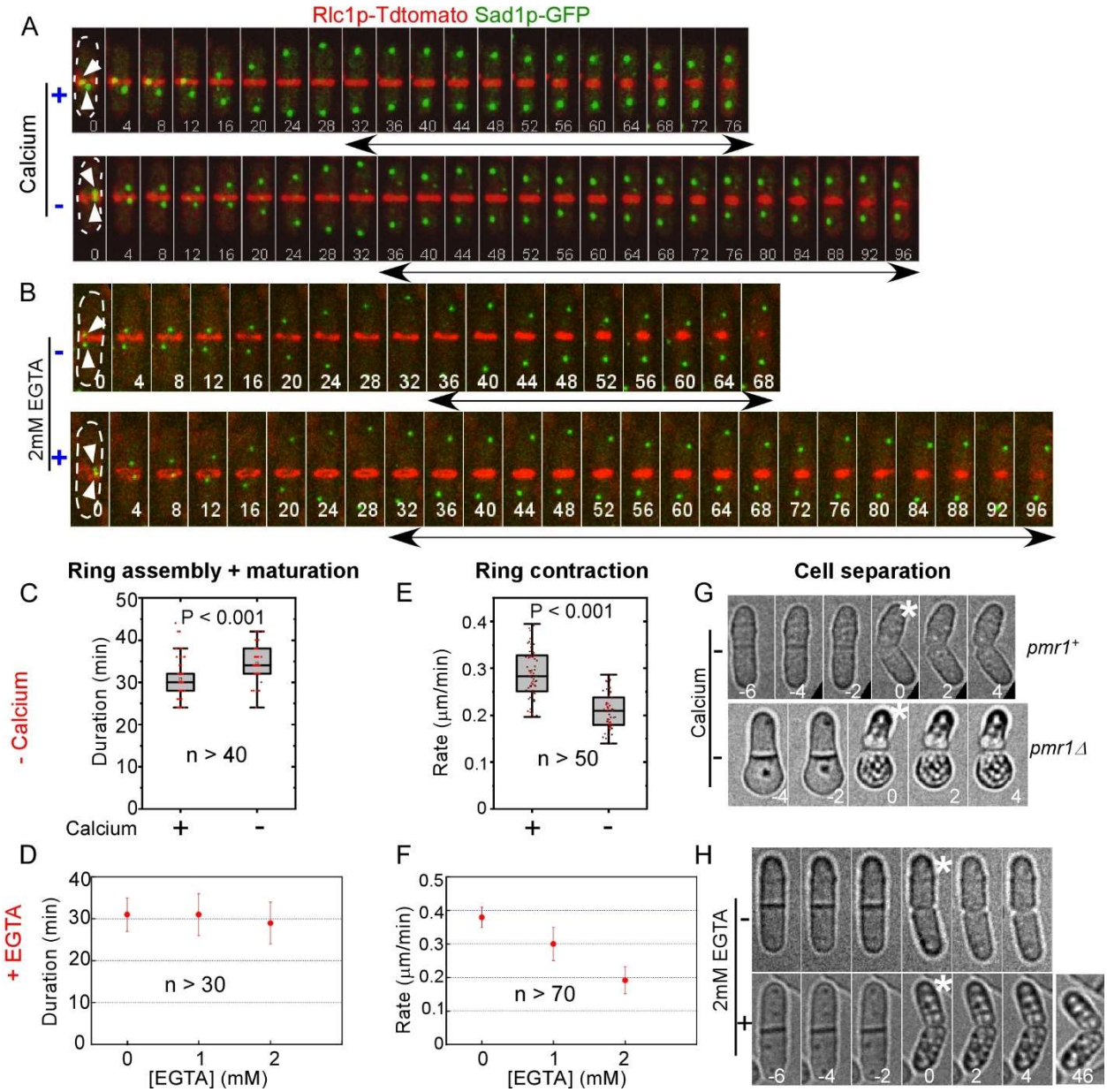

583

584 **Figure 9. Temporary depletion of extracellular calcium slows down the contractile ring**

585 **constriction and leads to daughter cell lysis. (A-F)** Temporary depletion of extracellular

586 calcium reduced the ring constriction rate, but it had little effect in the ring assembly and

587 maturation. **(A-B)** Temporary depletion of extracellular calcium slowed down the ring

588 constriction. Time-lapse micrographs of dividing cells expressed both Sad1-GFP (green) and

589 Rlc1p-tdTomato (red). Number: time in minutes after the separation of SPBs (arrowhead). Dash

590 line marks the outline of cells. **(A)** Cells in either regular EMM5s (top) or the calcium-free
591 EMM5s media (bottom). **(B)** Cells in either YE5s (top) or YE5s plus 2mM EGTA media
592 (bottom). **(C, D)** Duration of the ring assembly plus maturation. **(E, F)** The ring constriction
593 rates. **(G-H)** Temporary depletion of extracellular calcium increased the frequency of cell lysis
594 among the daughter cells. Time-lapse micrographs of separating cells. Number: time in minutes
595 after the cell separation. **(G)** The wild-type (top) or *pmr1Δ* (bottom) cells in the calcium-free
596 EMM5s media (bottom). Although the wild-type cells (n > 100) did not lysis during the
597 separation, 54% of the mutant cells lysed (asterisk) (n = 57). **(H)** The wild-type cells in either
598 YE5s (top) or YE5s plus 2mM EGTA (bottom). About 35% of daughter cells lysed after the
599 separation in the presence of EGTA (n > 100). Data is pooled from two biological repeats.
600

601 **Supplemental Materials**

602 **Supplemental Figure legends:**

Figure S1

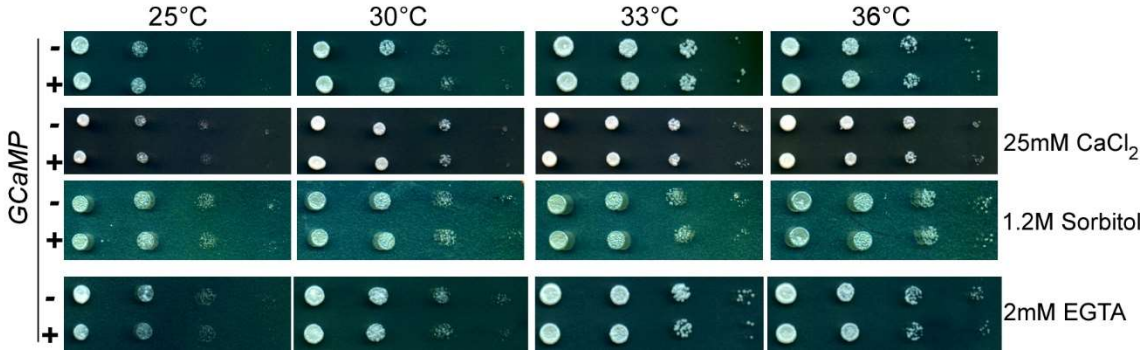

603

604 **Figure S1: Expression of GCaMP does not affect fission yeast growth. Related to Fig. 1.**

605 Ten-fold dilution series of both GCaMP-expressing and the wild-type cells. The cells were

606 inoculated at various temperatures on either YE5s (top), or YE5s plus 25mM $CaCl_2$, or YE5s

607 plus 1.2M sorbitol, or YE5s plus 2mM EGTA plates. GCaMP did not affect the yeast growth

608 under any of the conditions. Similar results were obtained in two biological repeats.

609

Figure S2

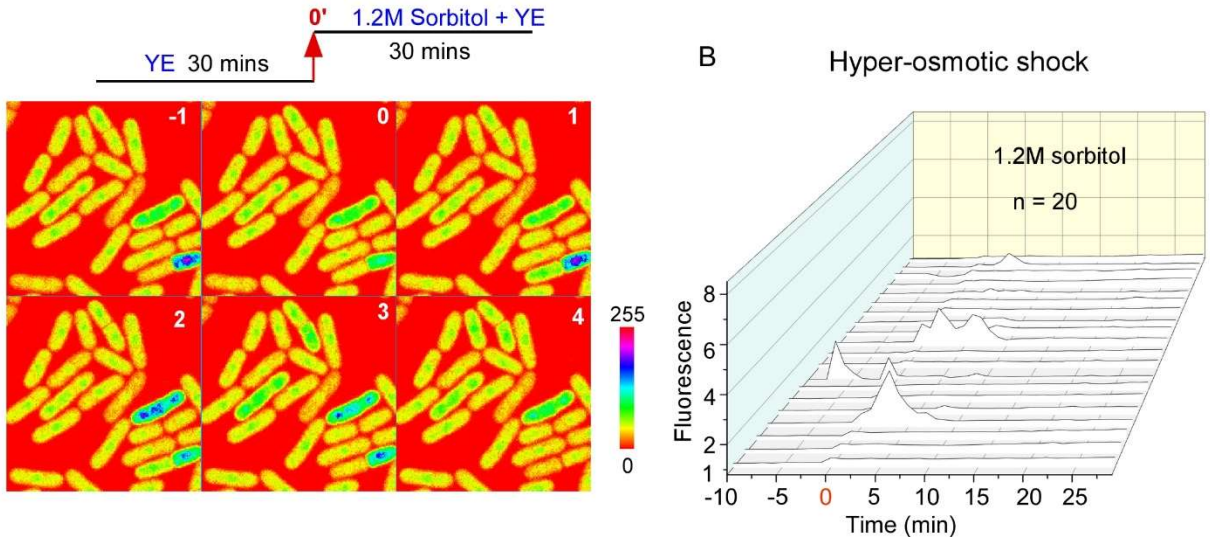

Figure S2: Hyper-osmotic shocks do not trigger calcium spikes. Related to Fig. 3. The cells were equilibrated with YE5s media for 30 mins in the microfluidic chamber before the infusion of YE5s plus 1.2M sorbitol (time zero). **(A)** Time-lapse micrographs (spectrum-colored) of the GCaMP expressing cells in a microfluidics chamber. Number: time in minutes after the shock. Unlike hypo-osmotic shock, hyper-osmotic shock did not trigger synchronized intracellular calcium spikes. Similar result was obtained in two biological repeats. **(B)** 3D line plots showing the time courses of the intracellular GCaMP fluorescence in twenty representative cells during the hyper-osmotic shock.

Figure S3

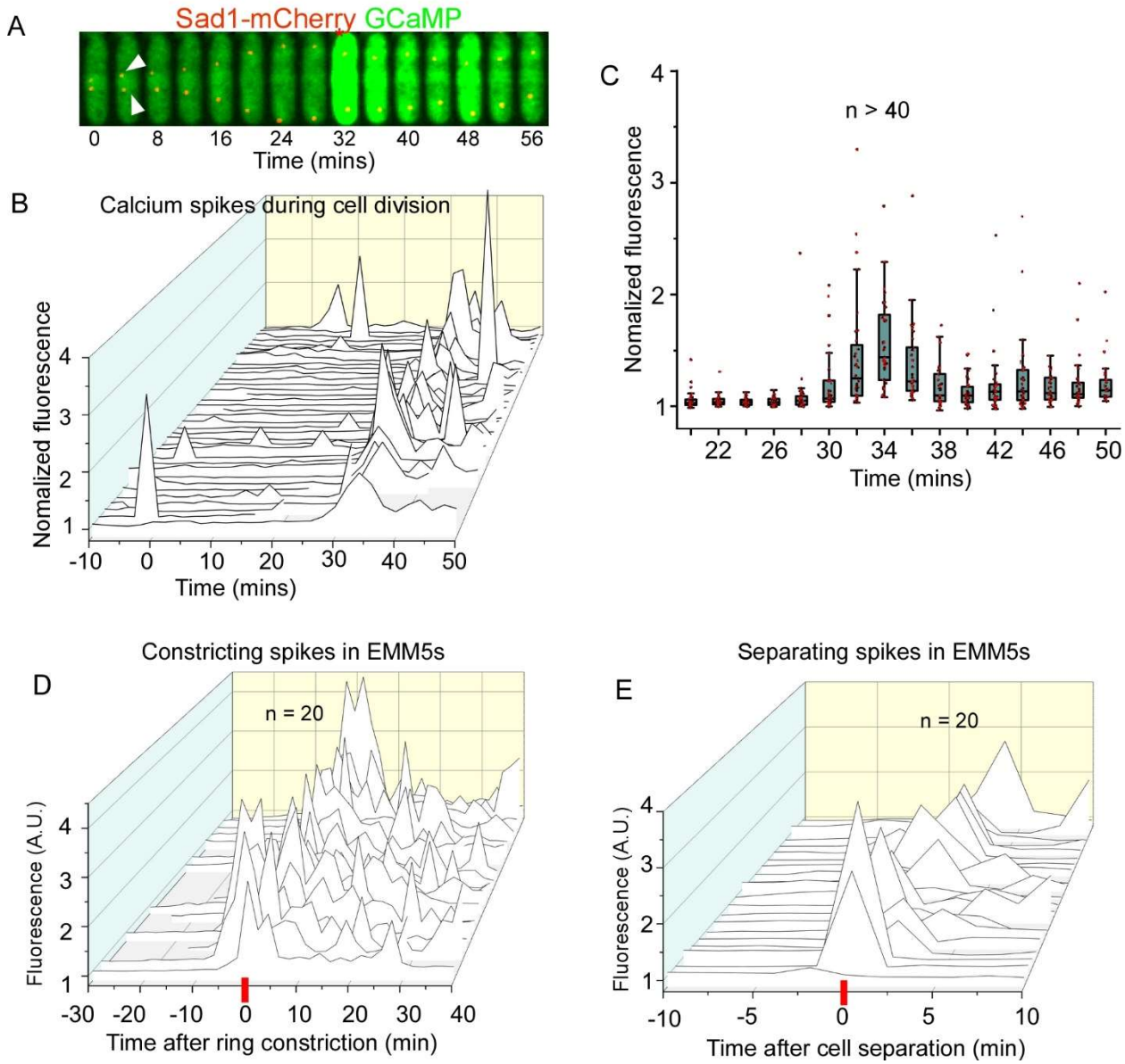

Figure S3: The calcium spikes in dividing cells. Related to Fig. 4, 5 and 6. (A-C) The intracellular calcium level increased during late mitosis. **(A)** Time-lapse fluorescence micrographs of a cell expressing both Sad1-mCherry (red) and GCaMP (green). Number: time in minutes after the SPB separation (arrowheads). Interval = 4 mins. The intracellular calcium level peaked at +32 mins (asterisk), at the start of telophase when two SPBs reached a maximum distance from each other. **(B)** 3D-line plots of the time courses of calcium level in mitotic cells (n = 36). The calcium level increased significantly starting ~ 30 mins after the separation of SPBs. **(C)** Box plots of the calcium level of those cells shown in B. The average calcium level peaked at +34 min, after the separation of the SPBs. The data was pooled from two biological repeats. **(D-E)** The cytokinetic calcium spikes in EMM5s media. 3D-line plots of the calcium level during the ring constriction (D) and cell separation (E). Similar constricting and separating spikes are found in these cells, as those inoculated in YE5s.

Figure S4

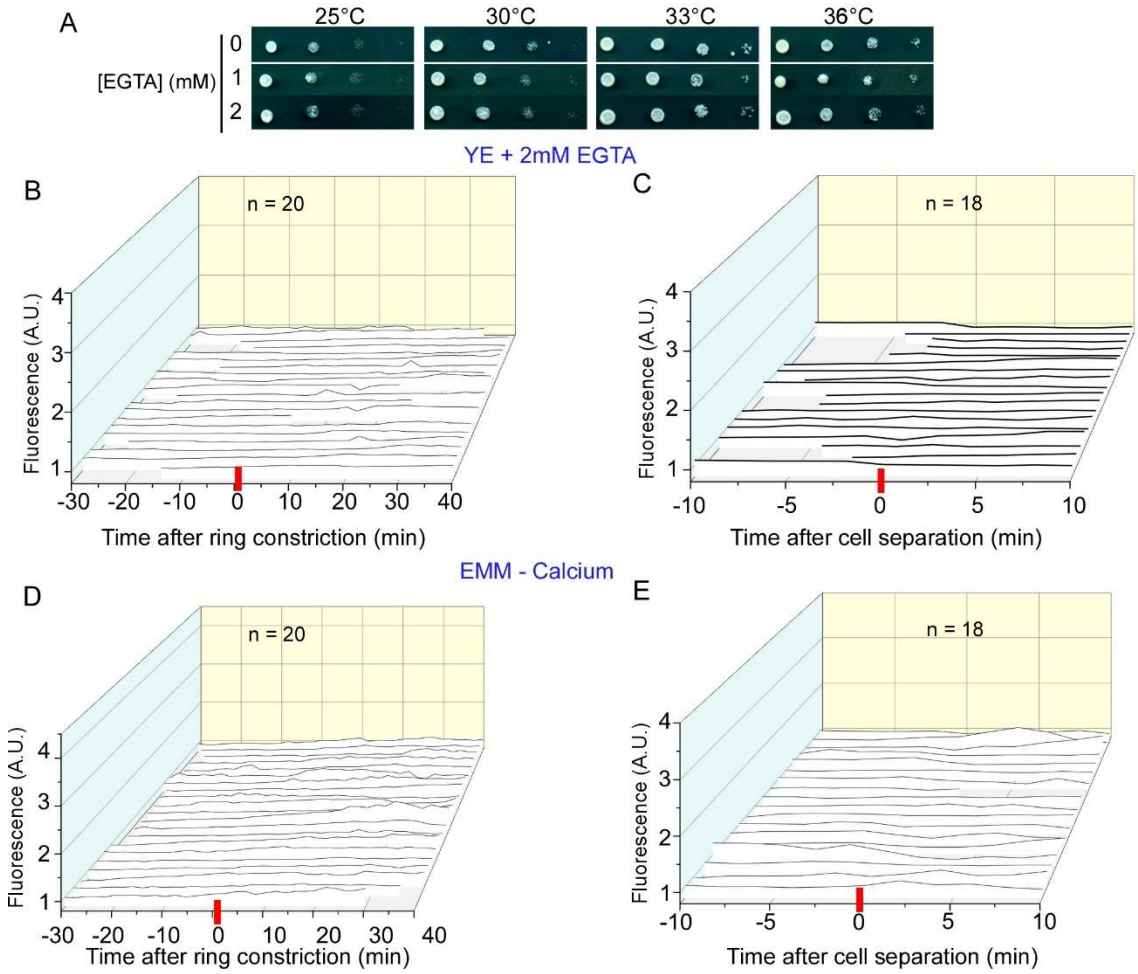

Figure S4: Depletion of extracellular calcium inhibits the cytokinetic calcium spikes. Related to Fig. 8. (A) Ten-fold dilution series of the wild-type yeast in YE5s plus 0-2 mM EGTA. Low concentration of EGTA didn't inhibit cell growth. **(B-E)** 3D-line plots showing the time courses of the calcium level of the representative cells in either YE5s plus 2mM EGTA (B-C) or the calcium-free EMM media (D-E) during either the ring closure (B and D) or the cell separation (C and E). Depletion of extracellular calcium inhibited the cytokinetic calcium spikes. The data is pooled from two biological repeats.

Figure S5

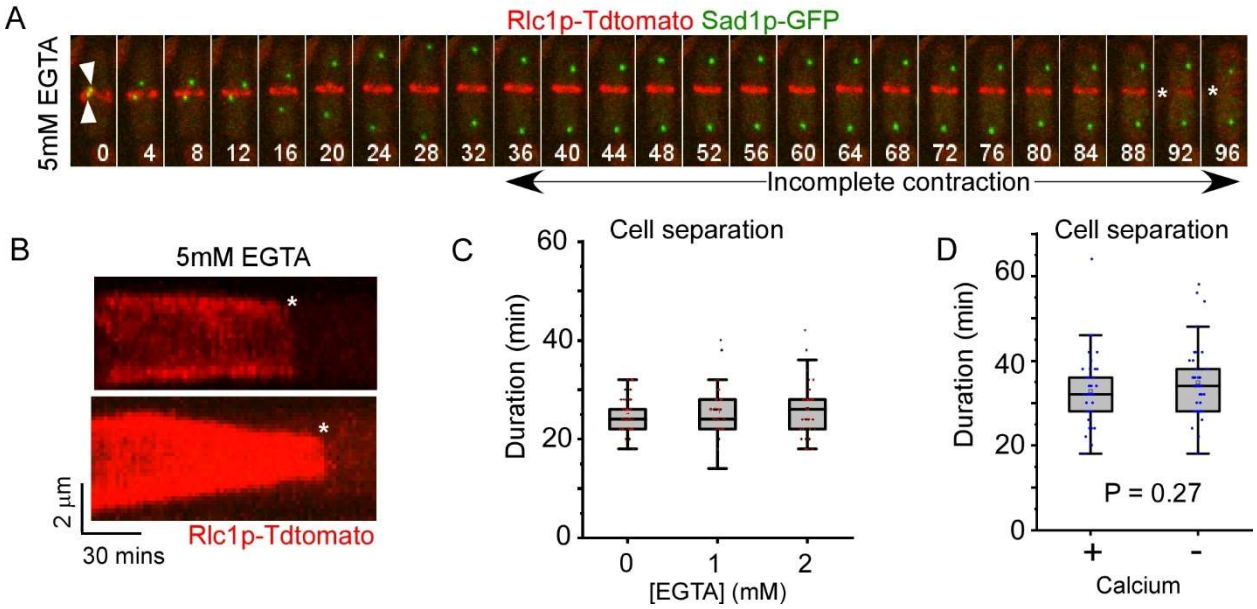

642

643 **Figure S5: Depletion of extracellular calcium slowed down the contractile ring constriction.**

644 **Related to Fig. 9. (A-B)** Depletion of calcium by 5 mM EGTA reduces the integrity of the

645 contractile ring. The cells expressed both Sad1p-GFP (green) and Rlc1p-tdTomato (red). **(A)**

646 Time-lapse micrographs of a cell in YE5s supplemented with EGTA. The contractile ring failed

647 to close completely before its disintegration (asterisk). Number: time in mins after the separation

648 of SPBs (arrowhead). **(B)** Kymographs of two contractile rings that failed to constrict completely

649 before their disintegration (asterisk). **(C-D)** Box plots showing the duration of cell separation

650 when extracellular calcium was depleted. The separation was not significantly delayed.

651

652 **Supplemental Tables:**

653 **Table 1: The list of yeast strains**

Strains	Genotype	Source
FY527	*h- leu1-32 ura4-D18 his3-D1 ade6-M216*	Lab stock
FY528	*h+ leu1-32 ura4-D18 his3-D1 ade6-M210*	Lab stock
QC-Y941	*h- leu1::KanMX6-Padh1-GCaMP6s*	This study
QC-Y989	*h- sad1-mCherry-NatMX6 leu1::Padh1-GCaMP6s-mCherry*	This study
QC-Y1004	*h+ rlc1-tdTomato-NatMX6 leu1::Padh1-GCaMP6s-mCherry*	This study
QC-Y1068	*h- leu1::Padh1-GCaMP6s-mCherry-ura4+*	This study
QC-Y274	*h- rlcl1-tdTomato-NatMX6 sad1-mGFP-KanMX6*	Lab stock
QC-Y1149	*h? pmr1::kanMX6 rlc1-tdTomato-natMX6 sad1-mEGFP-KanMX6*	This study

654 **Table 2: The list of DNA primers**

Primers	Sequence
P413	*TTTGGGAGGTGAGGCTTCTACCGCTGATATTACTAAGGCTGTTGTTGAAGA ACTTGAAAAAATTTTGTAAGAATTCGAGCTCGTTTAAAC*
P414	*ATGCGACACAATTAATCAATAAAAATTAGGTCAAATCAAATCATATGAATT TATTCTACATTAAACCCTAGCGGCCGCCAGCTGAAGCTT*
P415	*CCTTCTCCTTCGTTATGGTTTG*
P589	*TTAATTAAC-ATGGGTTCTCATCATCATCATC*
P590	*GGCGCGCC-TCACTTCGCTGTCATCATTTGTAC*
P668	*CAGGGACACGGAAGAAGAAATTA*
P416	*TCATAAAGTTGAACGGATGTCG*
P647	*CAGGGAAGCAGACATCGATGGGGATGGTCAGGTAAACTACGAAGAGTTTGTACAAATG ATGACAGCGAAGGTGAGCAAGGGCGAGGAGGA*
P648	*TTTATAACTTATTTAATAATAAAAATCATAAATCATAAGAAATTCGCTTATTTAGAAGTGGCGCGCC CTAGAATTCGAGCTCGTTTAAAC*

655 **Supplemental movies:**

656 **Movie S1: The calcium homeostasis of fission yeast reported by GCaMP-based imaging**

657 **(related to Fig. 2).** Time-lapse movie (60 mins) of GCaMP expressing cells in YE5s. Number:

658 time in minutes.

659 **Movie S2: The calcium spikes stimulated by hypo-osmotic shock (related to Fig. 3).** Time-

660 lapse movie of the GCaMP expressing cells in a microfluidic chamber. At time zero, the infusing

661 media was switched from YE5s plus 1.2M sorbitol to just YE5s. This hypo-osmotic shock (time

662 zero) triggered synchronized calcium transients. Number: time in minutes.

663 **Movie S3: The constricting calcium spike during cytokinesis (related to Fig. 4).** Time-lapse

664 movie of a dividing cell expressing both GCaMP (green) and Rlc1p-tdTomato (red). Number:
665 time in minutes. The calcium spike initiated as the ring constriction started (time zero) and
666 peaked at +2 min. Number: time in minutes.

667 **Movie S4: The separating calcium spike during cytokinesis (related to Fig. 5).** Time-lapse
668 movie of a GCaMP expressing cell during the cell separation. The calcium spike followed the
669 separation (time zero), oscillating between the two daughter cells. Number: time in minutes.

670 **Movie S5: Cytokinesis in the calcium depleted media (related to Fig. 9).** Time-lapse movie of
671 two cells in either YE5s (left) or YE5s plus 2mM EGTA (right). The cells expressed both
672 GCaMP (green) and Rlc1p-tdTomato (red). EGTA inhibited the cytokinetic calcium spikes. The
673 contractile ring constricted more slowly in the presence of EGTA. Number represents time in
674 minutes after the start of the ring constriction (time zero).

675 **References**

676 Abenza, J.F., E. Couturier, J. Dodgson, J. Dickmann, A. Chessel, J. Dumais, and R.E.C. Salas.
677 2015. Wall mechanics and exocytosis define the shape of growth domains in fission yeast.
678 *Nature communications*. 6:8400.
679 Arnold, J.M. 1975. effect of calcium in cytokinesis as demonstrated with ionophore A231ß7.
680 *Cytobiologie*. 11:1-9.
681 Atilgan, E., V. Magidson, A. Khodjakov, and F. Chang. 2015. Morphogenesis of the Fission Yeast
682 Cell through Cell Wall Expansion. *Curr Biol*. 25:2150-2157.
683 Bahler, J., J.Q. Wu, M.S. Longtine, N.G. Shah, A. McKenzie, 3rd, A.B. Steever, A. Wach, P.
684 Philippsen, and J.R. Pringle. 1998. Heterologous modules for efficient and versatile PCR-
685 based gene targeting in Schizosaccharomyces pombe. *Yeast (Chichester, England)*.
686 14:943-951.
687 Balasubramanian, M.K., D. McCollum, L. Chang, K.C. Wong, N.I. Naqvi, X. He, S. Sazer, and
688 K.L. Gould. 1998. Isolation and characterization of new fission yeast cytokinesis mutants.
689 *Genetics*. 149:1265-1275.
690 Batiza, A.F., T. Schulz, and P.H. Masson. 1996. Yeast respond to hypotonic shock with a calcium
691 pulse. *The Journal of biological chemistry*. 271:23357-23362.
692 Cadou, A., A. Couturier, C. Le Goff, L. Xie, J.R. Paulson, and X. Le Goff. 2013. The Kin1 kinase
693 and the calcineurin phosphatase cooperate to link actin ring assembly and septum synthesis
694 in fission yeast. *Biol Cell*. 105:129-148.
695 Carbo, N., N. Tarkowski, E.P. Ipina, S.P. Dawson, and P.S. Aguilar. 2017. Sexual pheromone
696 modulates the frequency of cytosolic Ca(2+) bursts in Saccharomyces cerevisiae.
697 *Molecular biology of the cell*. 28:501-510.
698 Chan, C.M., J.T. Aw, S.E. Webb, and A.L. Miller. 2016. SOCE proteins, STIM1 and Orai1, are
699 localized to the cleavage furrow during cytokinesis of the first and second cell division
700 cycles in zebrafish embryos. *Zygote*. 24:880-889.
701 Chan, C.M., Y. Chen, T.S. Hung, A.L. Miller, A.M. Shipley, and S.E. Webb. 2015. Inhibition of
702 SOCE disrupts cytokinesis in zebrafish embryos via inhibition of cleavage furrow
703 deepening. *The International journal of developmental biology*. 59:289-301.
704 Chang, D.C., and C. Meng. 1995. A localized elevation of cytosolic free calcium is associated with
705 cytokinesis in the zebrafish embryo. *The Journal of cell biology*. 131:1539-1545.
706 Chang, F., D. Drubin, and P. Nurse. 1997. cdc12p, a protein required for cytokinesis in fission
707 yeast, is a component of the cell division ring and interacts with profilin. *The Journal of*
708 *cell biology*. 137:169-182.
709 Chen, Q., and T.D. Pollard. 2011. Actin filament severing by cofilin is more important for
710 assembly than constriction of the cytokinetic contractile ring. *The Journal of cell biology*.
711 195:485-498.
712 Chen, Q., and T.D. Pollard. 2013. Actin filament severing by cofilin dismantles actin patches and
713 produces mother filaments for new patches. *Curr Biol*. 23:1154-1162.
714 Chen, T.W., T.J. Wardill, Y. Sun, S.R. Pulver, S.L. Renninger, A. Baohan, E.R. Schreiter, R.A.
715 Kerr, M.B. Orger, V. Jayaraman, L.L. Looger, K. Svoboda, and D.S. Kim. 2013.
716 Ultrasensitive fluorescent proteins for imaging neuronal activity. *Nature*. 499:295-300.
717 Clapham, D.E. 2007. Calcium signaling. *Cell*. 131:1047-1058.
718 Cortes, J.C., J. Ishiguro, A. Duran, and J.C. Ribas. 2002. Localization of the (1,3)beta-D-glucan
719 synthase catalytic subunit homologue Bgs1p/Cps1p from fission yeast suggests that it is
720 involved in septation, polarized growth, mating, spore wall formation and spore

721 germination. *Journal of cell science*. 115:4081-4096.
722 Cortes, J.C., R. Katoh-Fukui, K. Moto, J.C. Ribas, and J. Ishiguro. 2004. Schizosaccharomyces
723 pombe Pmr1p is essential for cell wall integrity and is required for polarized cell growth
724 and cytokinesis. *Eukaryot Cell*. 3:1124-1135.
725 Cortes, J.C., M. Sato, J. Munoz, M.B. Moreno, J.A. Clemente-Ramos, M. Ramos, H. Okada, M.
726 Osumi, A. Duran, and J.C. Ribas. 2012. Fission yeast Ags1 confers the essential septum
727 strength needed for safe gradual cell abscission. *The Journal of cell biology*. 198:637-656.
728 Courtemanche, N., T.D. Pollard, and Q. Chen. 2016. Avoiding artefacts when counting
729 polymerized actin in live cells with LifeAct fused to fluorescent proteins. *Nature cell*
730 *biology*. 18:676-683.
731 Craig, R., R. Smith, and J. Kendrick-Jones. 1983. Light-chain phosphorylation controls the
732 conformation of vertebrate non-muscle and smooth muscle myosin molecules. *Nature*.
733 302:436-439.
734 Deng, L., R. Sugiura, M. Takeuchi, M. Suzuki, H. Ebina, T. Takami, A. Koike, S. Iba, and T.
735 Kuno. 2006. Real-time monitoring of calcineurin activity in living cells: evidence for two
736 distinct Ca2+-dependent pathways in fission yeast. *Molecular biology of the cell*. 17:4790-
737 4800.
738 Denis, V., and M.S. Cyert. 2002. Internal Ca(2+) release in yeast is triggered by hypertonic shock
739 and mediated by a TRP channel homologue. *The Journal of cell biology*. 156:29-34.
740 Fluck, R.A., A.L. Miller, and L.F. Jaffe. 1991. Slow calcium waves accompany cytokinesis in
741 medaka fish eggs. *The Journal of cell biology*. 115:1259-1265.
742 Garcia Cortes, J.C., M. Ramos, M. Osumi, P. Perez, and J.C. Ribas. 2016. The Cell Biology of
743 Fission Yeast Septation. *Microbiology and molecular biology reviews : MMBR*. 80:779-
744 791.
745 Jaffe, L.F., and R. Creton. 1998. On the conservation of calcium wave speeds. *Cell calcium*. 24:1-
746 8.
747 Laplante, C., J. Berro, E. Karatekin, A. Hernandez-Leyva, R. Lee, and T.D. Pollard. 2015. Three
748 myosins contribute uniquely to the assembly and constriction of the fission yeast
749 cytokinetic contractile ring. *Curr Biol*. 25:1955-1965.
750 Liu, J., H. Wang, D. McCollum, and M.K. Balasubramanian. 1999. Drc1p/Cps1p, a 1,3-beta-
751 glucan synthase subunit, is essential for division septum assembly in Schizosaccharomyces
752 pombe. *Genetics*. 153:1193-1203.
753 Ma, Y., R. Sugiura, A. Koike, H. Ebina, S.O. Sio, and T. Kuno. 2011. Transient receptor potential
754 (TRP) and Cch1-Yam8 channels play key roles in the regulation of cytoplasmic Ca2+ in
755 fission yeast. *PLoS One*. 6:e22421.
756 Martin-Garcia, R., V. Arribas, P.M. Coll, M. Pinar, R.A. Viana, S.A. Rincon, J. Correa-Bordes,
757 J.C. Ribas, and P. Perez. 2018. Paxillin-Mediated Recruitment of Calcineurin to the
758 Contractile Ring Is Required for the Correct Progression of Cytokinesis in Fission Yeast.
759 *Cell reports*. 25:772-783 e774.
760 Miller, A.L., R.A. Fluck, J.A. McLaughlin, and L.F. Jaffe. 1993. Calcium buffer injections inhibit
761 cytokinesis in Xenopus eggs. *Journal of cell science*. 106 (Pt 2):523-534.
762 Mishra, M., J. Kashiwazaki, T. Takagi, R. Srinivasan, Y. Huang, M.K. Balasubramanian, and I.
763 Mabuchi. 2013. In vitro contraction of cytokinetic ring depends on myosin II but not on
764 actin dynamics. *Nature cell biology*. 15:853-859.
765 Mitchison, J.M., and P. Nurse. 1985. Growth in cell length in the fission yeast
766 Schizosaccharomyces pombe. *Journal of cell science*. 75:357-376.

767 Moser, M.J., M.R. Flory, and T.N. Davis. 1997. Calmodulin localizes to the spindle pole body of
768 Schizosaccharomyces pombe and performs an essential function in chromosome
769 segregation. *Journal of cell science*. 110 (Pt 15):1805-1812.
770 Munoz, J., J.C. Cortes, M. Sipiczki, M. Ramos, J.A. Clemente-Ramos, M.B. Moreno, I.M.
771 Martins, P. Perez, and J.C. Ribas. 2013. Extracellular cell wall beta(1,3)glucan is required
772 to couple septation to actomyosin ring contraction. *The Journal of cell biology*. 203:265-
773 282.
774 Nagai, T., A. Sawano, E.S. Park, and A. Miyawaki. 2001. Circularly permuted green fluorescent
775 proteins engineered to sense Ca2+. *Proceedings of the National Academy of Sciences of*
776 *the United States of America*. 98:3197-3202.
777 Nakai, J., M. Ohkura, and K. Imoto. 2001. A high signal-to-noise Ca(2+) probe composed of a
778 single green fluorescent protein. *Nat Biotechnol*. 19:137-141.
779 Nishimura, J., R.A. Khalil, J.P. Drenth, and C. van Breemen. 1990. Evidence for increased
780 myofilament Ca2+ sensitivity in norepinephrine-activated vascular smooth muscle. *The*
781 *American journal of physiology*. 259:H2-8.
782 Noguchi, T., and I. Mabuchi. 2002. Localized calcium signals along the cleavage furrow of the
783 Xenopus egg are not involved in cytokinesis. *Molecular biology of the cell*. 13:1263-1273.
784 Pollard, T.D., and J.Q. Wu. 2010. Understanding cytokinesis: lessons from fission yeast. *Nature*
785 *reviews*. 11:149-155.
786 Proctor, S.A., N. Minc, A. Boudaoud, and F. Chang. 2012. Contributions of turgor pressure, the
787 contractile ring, and septum assembly to forces in cytokinesis in fission yeast. *Curr Biol*.
788 22:1601-1608.
789 Scholey, J.M., K.A. Taylor, and J. Kendrick-Jones. 1980. Regulation of non-muscle myosin
790 assembly by calmodulin-dependent light chain kinase. *Nature*. 287:233-235.
791 Sipiczki, M. 2007. Splitting of the fission yeast septum. *FEMS yeast research*. 7:761-770.
792 Snow, P., and R. Nuccitelli. 1993. Calcium buffer injections delay cleavage in Xenopus laevis
793 blastomeres. *The Journal of cell biology*. 122:387-394.
794 Takeda, T., and M. Yamamoto. 1987. Analysis and in vivo disruption of the gene coding for
795 calmodulin in Schizosaccharomyces pombe. *Proceedings of the National Academy of*
796 *Sciences of the United States of America*. 84:3580-3584.
797 Thevenaz, P., U.E. Ruttimann, and M. Unser. 1998. A pyramid approach to subpixel registration
798 based on intensity. *IEEE Trans Image Process*. 7:27-41.
799 Tian, L., S.A. Hires, T. Mao, D. Huber, M.E. Chiappe, S.H. Chalasani, L. Petreanu, J. Akerboom,
800 S.A. McKinney, E.R. Schreiter, C.I. Bargmann, V. Jayaraman, K. Svoboda, and L.L.
801 Looger. 2009. Imaging neural activity in worms, flies and mice with improved GCaMP
802 calcium indicators. *Nat Methods*. 6:875-881.
803 Wu, J.Q., J.R. Kuhn, D.R. Kovar, and T.D. Pollard. 2003. Spatial and temporal pathway for
804 assembly and constriction of the contractile ring in fission yeast cytokinesis.
805 *Developmental cell*. 5:723-734.
806 Yoshida, T., T. Toda, and M. Yanagida. 1994. A calcineurin-like gene ppb1+ in fission yeast:
807 mutant defects in cytokinesis, cell polarity, mating and spindle pole body positioning.
808 *Journal of cell science*. 107 (Pt 7):1725-1735.
809